

Unusual Deprotonated Alkynyl Hydrogen Bonding in Metal-Supported Hydrocarbon Assembly

Yi-Qi Zhang,^{†,⊥} Jonas Björk,^{‡,⊥} Peter Weber,[†] Raphael Hellwig,[†] Katharina Diller,[†] Anthoula C. Papageorgiou,[†] Seung Cheol Oh,[†] Sybille Fischer,[†] Francesco Allegretti,[†] Svetlana Klyatskaya,[§] Mario Ruben,^{§,||} Johannes V. Barth,[†] and Florian Klappenberger^{*,†}

[†]Physik Department E20, Technische Universität München, 85748 Garching, Germany

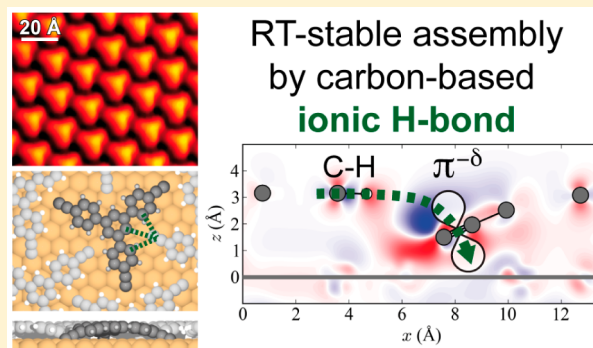
[‡]Department of Physics, Chemistry and Biology (IFM), Linköping University, 58183 Linköping, Sweden

[§]Institute of Nanotechnology (INT), Karlsruhe Institute of Technology (KIT), 76344 Eggenstein-Leopoldshafen, Germany

^{||}IPCMS-CNRS, Université de Strasbourg, 23 rue de Loess, 67034 Strasbourg, France

Supporting Information

ABSTRACT: We demonstrate that terminal alkynyl moieties represent powerful functional groups for driving thermally stable, on-surface supramolecular structure formation on a reactive substrate. Through a combination of scanning tunneling microscopy, X-ray photoelectron spectroscopy, near-edge X-ray absorption-fine-structure spectroscopy and density functional theory calculations, we investigate the molecule–surface interaction and self-assembly of two prototypical hydrocarbon species on Cu(111). For 1,3,5-tris(4-ethynylphenyl)benzene (Ext-TEB) adsorption at low temperature (200 K) results in nonassembling, conformationally adapted intact species. Deprotonation of the terminal alkyne moieties, taking place at temperatures ranging from 300 to 350 K, triggers the formation of room-temperature stable, close-packed supramolecular islands. Through DFT calculations, the stabilizing interaction is identified as a trifurcated ionic C–H $\cdots\pi$ ^{−δ} hydrogen bonding between the π -system of the ionic alkynyl groups and methine moieties of nearby benzene rings, providing an energy gain of 0.26 eV/molecule upon network formation. Robust assemblies result from the combination of this weak directional attraction with the strong surface anchoring also provided by the alkynyl groups. The generality of this novel ionic hydrogen-bonding type is demonstrated by the observation of low-dimensional assemblies of 9,10-diethynyl-anthracene on the same surface, consistently explained with the same type of interaction.



INTRODUCTION

Understanding and controlling supported molecular architectures is of fundamental importance for fabricating molecular device elements through the bottom-up approach.^{1–7} Hydrogen bonding, which provides selectivity and directionality combined with error corrective processes, has been successfully employed in the noncovalent synthesis of low-dimensional nanostructures.^{8–11} Although the strength of a single conventional H-bond between neutral molecules is rather weak² compared to that of a covalent bond¹² and metal–ligand interactions,^{2,12} it can be augmented¹³ when the net charges of one or both of the H-bond partners deviate from zero. This type of hydrogen bond, which is in the transition region to the ionic interaction, is classified as the ionic hydrogen bond (IHB),^{13,14} whereby the relevant partial charge can be contributed either from the proton donor D or the proton acceptor A, yielding D–H⁺ \cdots A-type and D–H \cdots A[−]-type interactions.¹³ IHBs have been recognized as the key ingredient in such diverse topics as molecular crystal engineering,¹⁵ protein folding,^{16,17} proton-coupled electron transfer,¹⁸ and

biomolecular recognition.¹⁹ Also recent studies of surface-confined supramolecular self-assembly under ultrahigh vacuum conditions appreciated their important roles for nanoscale architectures. These studies notably revealed that on metal surfaces, the carboxyl^{20–23} and hydroxyl functional groups^{24,25} can be thermally dehydrogenated resulting in charged carboxylate and carbonyl moieties, mediating the formation of room-temperature stable supramolecular structures with IHBs of the CH \cdots O[−]-type^{20–22} and OH \cdots O[−]-type.^{22–25} Another notable example is the assembly of L-methionine on Ag(111): the molecules are in a zwitterionic state on the surface, and the two oppositely charged functional groups account for a robust mesoscopic ordering of nanogratings.²⁶ Analysis of the observed situations^{22,23,26,27} reveals that with the complex surface chemistry and charge-screening capabilities of the metal support, novel possibilities arise for bottom-up construction of

Received: March 27, 2015

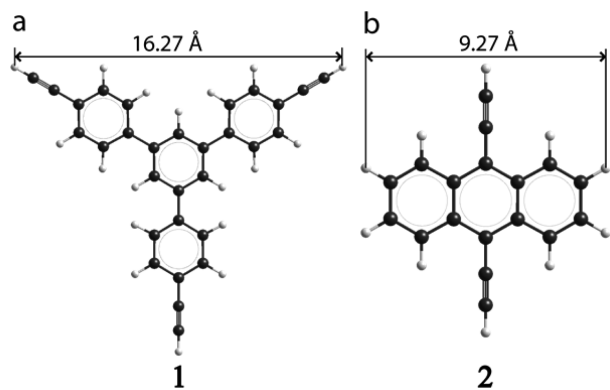
Revised: April 4, 2015

Published: April 8, 2015

nanoarchitectures in contrast to solvent and bulk environments where stabilizing counterions interfere.^{13,23}

Here we demonstrate how the surface-mediated formation and stabilization of ionic alkynyl groups provides the basis for a novel IHB-type with significant potential for bottom-up construction of future functional nanostructures because of the observed room-temperature stability of the assembled structures. It has been shown recently that terminal alkyne-functionalized hydrocarbon species can form flat-lying clusters²⁸ and long-range ordered supramolecular sheets^{29,30} on noble metal surfaces at low temperature through weak hydrogen bonding (i.e., C–H $\cdots\pi$ bonds), where the alkyne groups simultaneously act as proton donors (R–C \equiv C–H moiety) and proton acceptors (π system in the carbon–carbon triple bond, R–C \equiv C–H).³¹ However, the energy gain by network formation was only 0.11 eV/molecule.²⁹ In the present study, the behavior of 1,3,5-tris(4-ethynylphenyl)benzene (Ext-TEB, **1**, Scheme 1a) on the Cu(111) surface was investigated

Scheme 1. Ball-and-Stick Models of Employed Molecules: (a) 1,3,5-Tris(4-ethynylphenyl)benzene (Ext-TEB, **1**) and (b) 9,10-Diethynyl-anthracene (DEAN, **2**)^a



^aC and H atoms are depicted in black and white, respectively.

by means of scanning tunneling microscopy (STM), synchrotron-based X-ray photoelectron spectroscopy (XPS), near-edge X-ray absorption-fine-structure (NEXAFS) spectroscopy and density functional theory (DFT) simulations. We found that deprotonation of the terminal alkynes is initiated above 300 K, resulting in room-temperature stable structures in which the partially negatively charged alkynyl groups (δ^- -C \equiv C–R) interact strongly with both the surface and the neighboring aromatic rings. This new binding motif is identified as a trifurcated ionic C–H $\cdots\pi$ $^{\delta^-}$ hydrogen bond, providing an energy gain of 0.26 eV/molecule upon network formation. The generality of this novel IHB is demonstrated by employing 9,10-diethynyl-anthracene (DEAN, **2**), which self-assembles into molecular chains and trimeric clusters on Cu(111) after annealing above 300 K, with a bonding motif that can be rationalized by the same type of interaction.

RESULTS AND DISCUSSION

STM Studies. To study the behavior of terminal alkynes on Cu(111), we employed Ext-TEB, Scheme 1. The STM image in Figure 1a shows a submonolayer of Ext-TEB on Cu(111) (annealing temperature, $T_{\text{ann}} = 200$ K): individual molecules appear as triangular protrusions (inset of Figure 1a) and no ordered arrangement can be observed. The uniform appearance

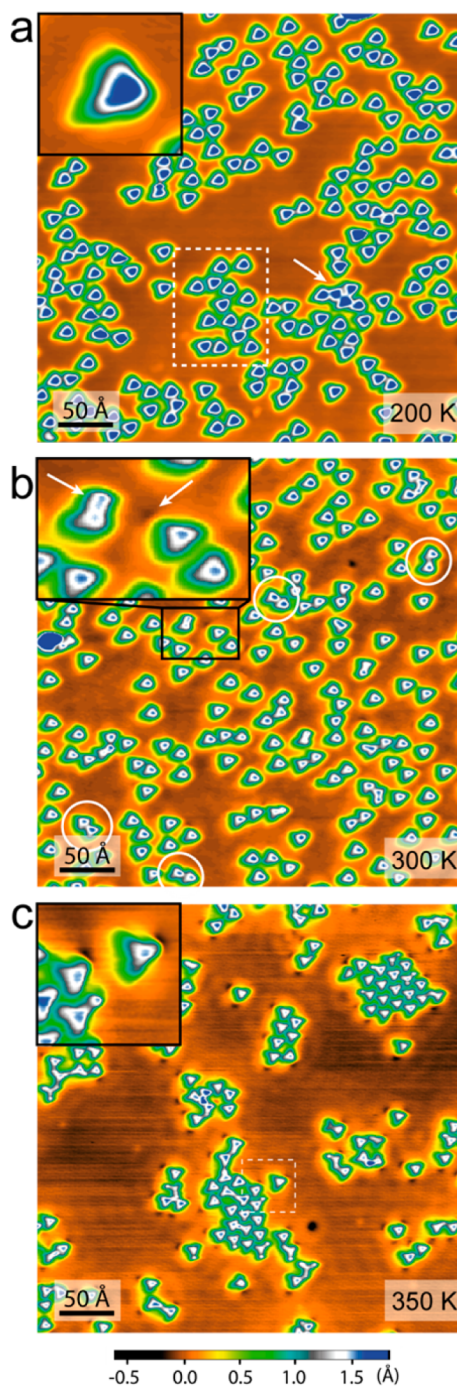


Figure 1. STM images (5.5 K) of the Ext-TEB molecules on Cu(111) following different thermal treatments. All images are displayed with the same apparent height color scale as shown. (a) $T_{\text{ann}} = 200$ K; the inset shows an isolated Ext-TEB molecule with a triangular shape and no depression around the alkyne groups (located at the triangle apexes). ($U_b = -1$ V, $I_t = 0.1$ nA.) (b) $T_{\text{ann}} = 300$ K; zoom-in: a depression and a protrusion in the immediate vicinity of the terminal alkynes are indicated by white arrows. ($U_b = -0.92$ V, $I_t = 0.13$ nA.) (c) $T_{\text{ann}} = 350$ K; the inset shows two depressions and a protrusion existing around the alkynyl groups. ($U_b = -0.9$ V, $I_t = 0.15$ nA.)

of the separated entities hints to the presence of intact species. The irregular positioning of the adsorbates indicates a much stronger surface interaction in comparison to Ag(111), where long-range ordered domains exist for similar preparation conditions.²⁹ The presence of a small number of molecular

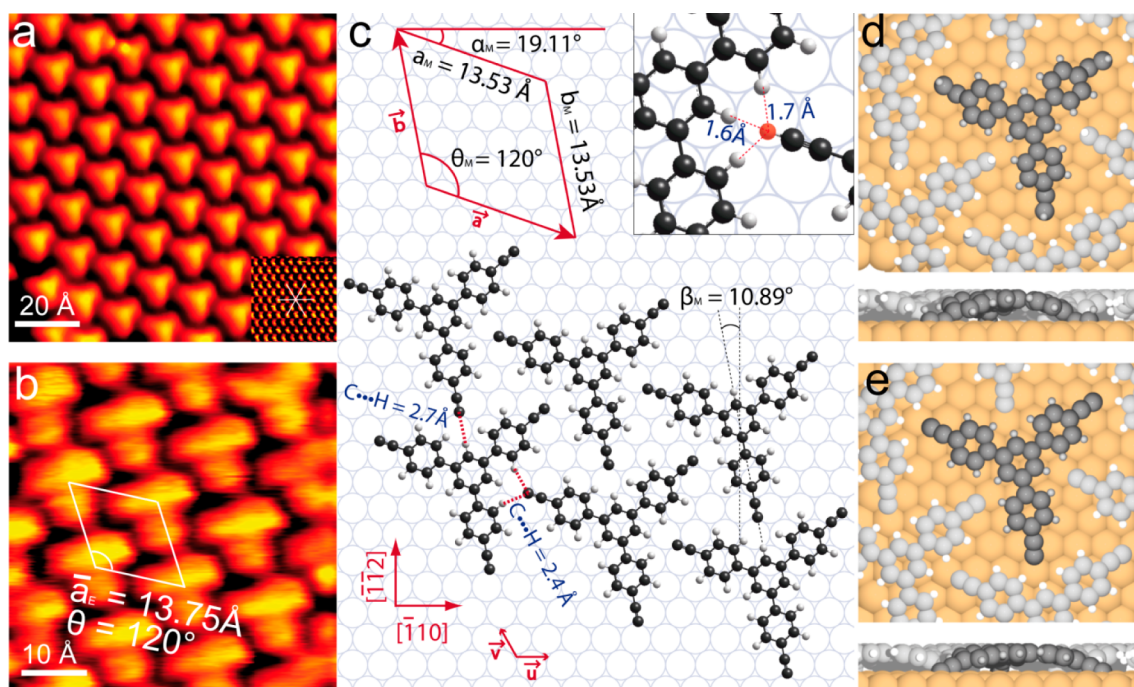


Figure 2. (a) STM image of Ext-TEB molecular island on Cu(111) formed by annealing at 350 K. ($U_b = 0.97$ V, $I_t = 0.16$ nA, $T_{STM} = 5.5$ K). The inset shows the respective atomically resolved Cu(111) surface. (b) STM image of the molecular island recorded at room temperature. ($U_b = -0.5$ V, $I_t = 1.0$ nA, $T_{STM} = 300$ K). The sample was prepared on a different Cu(111) crystal and scanned with a different STM setup. Thus, the close-packed directions of this crystal deviate from those in (a). (c) A simplified model of the molecular superstructure, using planar gas phase model calculated by HYPERCHEM. The inset shows the distances between the hypothetical terminal H atom (red) and the neighboring H atoms. Top and side views of DFT-optimized adsorption geometries of (d) intact molecular network and (e) deprotonated molecular network.

clusters (white arrow) is consistent with a hit-and-stick adsorption behavior. For the majority of the molecules, the white contour regions remain isolated, and the rounded corners of the triangles point toward the corners of neighboring molecules (highlighted with dashed rectangle). Such schemes are consistent with weak attractive interaction between intact ethynyl groups ($\text{H}-\text{C}\equiv\text{C}-\text{R}$),^{28,29,32,33} as depicted in Figure S1a of the Supporting Information. After annealing the sample at 300 K (Figure 1b), the irregular clustering is suppressed, and concomitantly the most probable molecule–molecule distance is increased (cf. Figure S2 of the Supporting Information), which indicates repulsive intermolecular interactions^{34–37} and kinetically limited growth below 300 K. In addition to the isolated units, a few examples of dimers are visible (Figure 1b, white circles), where one corner of one molecule points toward the center of the adjacent molecule. The change of the relative placement suggests a new interaction scheme for these dimers. Additionally, in rare cases, a depression next to a triangle corner can be recognized (inset of Figure 1b and Figure S2b of the Supporting Information), in contrast to the previous case ($T_{\text{ann}} = 200$ K). The copper surface is known for its potential for H abstraction.^{20,38–42} Furthermore, similar depressions have been observed at the vicinity of the carboxylate groups of deprotonated 4-[*trans*-2-(pyrid-4-yl-vinyl)] benzoic acid molecules on Cu(111)^{43,44} and were attributed to the negative charging of the carboxylate group through metal–organic bond formation.⁴³ Similarly, we attribute the emergence of the depressions to the H-abstraction and formation of ionic alkynyl groups, and this will be discussed and verified in detail later in this paper. It is worth noting that on the Ag(111) surface, no depressions were observed at the Ext-TEB legs after heating the substrate to 300 K. However, such features can be induced on

this less reactive substrate (Figure S3 of the Supporting Information) by applying protocols similar to those used for tip-induced deprotonation in related systems.^{45,46}

Annealing the sample at 350 K induces several changes in the appearance of the assembly of **1** (Figure 1c). First, small patches of regular molecular islands are formed in which adjacent molecules adopt a similar arrangement as in the afore-described dimers. Second, the percentage of deprotonated functional groups is strongly increased (Figure S2b of the Supporting Information). The concurrent emergence of the regular superstructure and the depressions suggests that the deprotonation of the molecules is a requirement for the formation of the dense-packed islands. At this stage, it is however unclear if only the peripheral moieties are ionic alkynyls or if alkyne groups at the interior part of the islands have lost their hydrogens as well. Aside the depressions, sometimes protrusions appear next to the legs of the molecules (see inset of Figure 1c). Analyzing the geometry of these features by superposition of models of planar molecules (Figure S1b of the Supporting Information) shows that the protrusion is located at the carbon–carbon triple bond ($\text{C}\equiv\text{C}$). This could imply π -bonded Cu-acetylide organometallic structures in contrast to a more intuitive σ -bonded situation. Possibly, the Cu atom is located on top of the alkynyl group. Unraveling the real geometry of this species requires further detailed investigations going beyond the scope of this work, though less well resolved, similar protrusions were already present in a minor number of adsorbates for $T_{\text{ann}} = 300$ K (see inset of Figure 1b, left arrow).

Next, we investigate the supramolecular domains in more detail to disentangle their chemical nature and the driving forces underlying their formation. By increasing the molecular

coverage, larger islands evolve, exhibiting a highly ordered, close-packed arrangement (Figure 2a), whose superstructure is very different from the one observed on Ag(111).²⁹ The lengths of the unit cell vectors, obtained from low-temperature STM measurements, are $|\mathbf{a}_E| = |\mathbf{b}_E| = 13.2 \pm 0.6 \text{ \AA}$, with an angle $\theta_E = 121 \pm 2^\circ$ in between. The angle α_E between the vector \mathbf{a} and the Cu [110] direction is $20.5 \pm 0.4^\circ$. The angle β specifying the azimuthal orientation of the molecules relative to the Cu[112] direction is obtained by superimposing a HYPERCHEM optimized ball-and-stick model (gas phase) onto the STM image, which gives $\beta_E = 10 \pm 2^\circ$. STM measurements revealed that this supramolecular lattice is stable at room temperature (Figure 2b). It is noteworthy that the island formation does not result from space-limitations due to a coverage near to monolayer saturation, as can be seen in the images shown in Figure S4 of the Supporting Information, demonstrating the applicability of deprotonated terminal alkynes for the engineering of robust stable nanostructures.

Guided by the experimental values, the model of the molecular network can be constructed as depicted in Figure 2c, where a planar conformation of the tectons is assumed. With the definition of the primitive vectors of the Cu(111) substrate, the elementary cell can be written in matrix representation as

$$\begin{pmatrix} \vec{a} \\ \vec{b} \end{pmatrix} = \begin{pmatrix} 4 & -2 \\ 2 & 6 \end{pmatrix} \begin{pmatrix} \vec{u} \\ \vec{v} \end{pmatrix}$$

Given the nearest-neighbor distance of 2.556 Å for the Cu(111) surface, we obtain a commensurate superstructure with $|\mathbf{a}_M| = |\mathbf{b}_M| = 13.53 \text{ \AA}$, $\theta_M = 120^\circ$, $\alpha_M = 19.11^\circ$, and $\beta_M = 10.9^\circ$.

Assuming a flat-lying geometry of each molecule, the model depicted in Figure 2c suggests that all the molecules within the network are deprotonated at all three alkyne groups. An alternative explanation assuming protonated terminal alkynes (inset in Figure 2c) would imply rather short distances, ≈ 1.6 – 1.7 \AA , between the hypothetical terminal H atom (highlighted in red) and the H atoms from neighboring phenyl rings. The expected repulsive interaction from entering the Pauli regime renders this model unreasonable. In contrast, for deprotonated alkynes, the distances between terminal C atoms and the neighboring aromatic ring hydrogens (red dotted lines in Figure 2c) are 2.4 and 2.7 Å, respectively, which correspond to the typical distances for hydrogen bonding.² However, with the indications for strong substrate interaction discussed above, distorted geometries of the organic building-blocks from conformational adaptation upon adsorption seem probable,^{47–50} making the detailed explanation of the supramolecular structure a nontrivial problem.

To get deeper insight into the surface-influenced chemical state of the tectons and their interactions, we carried out extensive DFT calculations (see Methods). First, isolated intact and triply deprotonated molecules were geometry-optimized on the Cu(111) surface slabs (Figure S5a of the Supporting Information). In both cases, strongly deformed conformations were obtained, with a significant electron charge transfer from the substrate to the molecules according to Bader charge analysis (Figure S5b of the Supporting Information). The negative charging of the intact molecule explains the intermolecular repulsion indicated by the experimental observations (cf. Figure 1 (panels a and b) and Figure S2a of the Supporting Information). Moreover, the negatively charged regions are localized at the alkyne and alkynyl groups for the

intact and deprotonated species, respectively (Figure S5b of the Supporting Information). Furthermore, STM image simulations show depressions next to the corners of the triangular appearance of the deprotonated tectons, but not for the intact ones (Figure S5c of the Supporting Information), supporting the proposed H abstraction upon annealing. Additionally, by comparing the STM data with simulated STM images of different bias voltages, a significantly better agreement is found in the latter case (Figure S6 of the Supporting Information). Finally, calculations were also performed for networks consisting of either intact (Figure 2d) or deprotonated (Figure 2e) species, where the unit cell was defined according to the model shown in Figure 2c. As discussed in more detail below, an energy gain of $-0.04 \text{ eV/molecule}$ and 0.26 eV/molecule upon network formation was found for the intact (Figure 2d) and the deprotonated (Figure 2e) case, respectively. Altogether, the modeling indicates that for the dense-packed islands, the functional groups at the periphery as well as inside the domains are deprotonated. The theoretical energy considerations agree with the absence of island formation for intact molecules and demonstrate that the terminal alkynyl moieties provide a rather weak but decisive driving force directing the self-assembly of the hydrocarbon species.

XPS. The deprotonation scenario of Ext-TEB on Cu(111) was investigated by XPS measurements, complementing the STM and DFT investigations. Figure 3a shows the C 1s

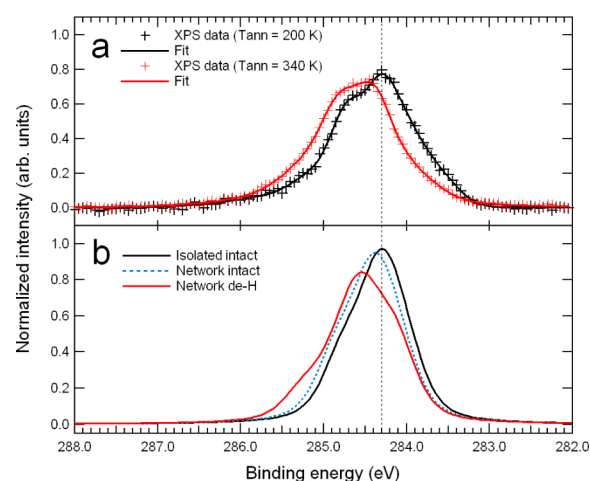


Figure 3. (a) Experimental XPS data of the C 1s region of Ext-TEB on Cu(111), prepared by depositing molecules onto Cu(111) held at 200 K (black curve) and annealing at 340 K (red curve). (b) DFT-simulated lineshapes of an isolated intact molecule (solid black line), a deprotonated network (solid red line), and an intact network (dashed blue line) on Cu(111). The reference energy is 284.18 eV. The core-level shifts of the C atoms are shown in Figure S7 of the Supporting Information.

spectrum of a sample with a coverage of 1 slightly below one monolayer, prepared and measured at a substrate temperature of 200 K. A double-peak structure is present with maximum intensity at an energy of 284.3 eV, followed by a shoulder at a higher binding energy (284.7 eV). After annealing to 340 K, the intensity maximum of the main peak slightly shifts to a higher binding energy of $E_b = 284.5 \text{ eV}$ and the shoulder becomes more intense, almost reaching the level of the main feature (Figure 3a). Since the adsorption geometry in the deprotonated network (Figure 2e) suggests the formation of σ -bond like Cu-acetylide moieties (with atoms from the first substrate layer)

and typical metal-acetylide binding energies are between 283 and 284 eV,^{51–53} the general shift to higher E_b seems at first glance to contradict the proposed deprotonation scenario.

For a more detailed understanding of the actual situation, XPS spectra were simulated by calculating the relative core-level shifts of each carbon atom for the DFT-optimized adsorption geometries of an isolated intact molecule, the deprotonated network, and the intact network (Figure S7 of the Supporting Information). For obtaining the spectra depicted in Figure 3b, a reference energy of 284.18 eV, obtained by best fitting the isolated intact spectra to the experimental 200 K data, was used in all cases, and Voigt peaks for each carbon atom were summed taking the calculated relative core-level shifts into account. A comparison of the spectrum of the isolated intact molecule (Figure 3b, black line) with the case of the deprotonated network (Figure 3b, red line) not only indicates that the acetylide low-energy signature does not appear but also yields changes very similar to the experimental ones, namely a slight upshift of E_b of the intensity maximum and a more intense high energy shoulder. In contrast, the changes derived for the intact network model (blue dashed line) are only marginal and would most likely not be resolved in experiments conducted with the available resolution, especially when considering that a mixture of deprotonated and intact molecules adsorbing on the surface may cause additional broadening. Thus, the observed changes of XPS characteristics induced by annealing agree with the deprotonation-driven assembly scenario indicated by the STM and DFT findings.

NEXAFS. To assess the conformational adaption of adsorbed **1** within the different environments, near-edge X-ray absorption-fine-structure (NEXAFS) measurements were carried out. Multilayer films were grown on Ag(111) as a reference, and the obtained spectra were analyzed with the help of the StoBe⁵⁴ package, as described in the Supporting Information. It has been demonstrated that the StoBe analysis provides valuable insight into NEXAFS signatures of complex molecules as long as the substrate interaction remains negligible.^{50,55–57} As detailed in Figure S8 of the Supporting Information, the case of the Ext-TEB multilayer can again be well understood by this approach. For an estimate of the surface influence, we then measured a sample ($T_{\text{meas}} = 135$ K) with near-to-monolayer coverage grown on Ag(111) at 300 K. Under such conditions, the surface is characterized by mainly intact species assembled in regular domains.^{29,51} Figure 4a shows the C K-edge NEXAFS spectra for three different incidence angles, θ . The changes of the magic angle spectra ($\theta = 53^\circ$, red line) with respect to the multilayer case are only marginal, indicating physisorption affecting only the orientation of the molecule. According to our StoBe analysis, the peaks at 285.2 and 286 eV are dominantly related to π^* resonances of the phenyl rings and the alkyne moieties, respectively (Figure S8 of the Supporting Information). Consistently with the orientation of the final orbitals being perpendicular to and within the surface plane for phenyls and alkynes, respectively, opposite angle-dependences are present for the two peaks. The evaluation of the phenyl angle-dependence (Figure S9a of the Supporting Information) indicates a flat adsorption geometry consistent with the DFT calculations depicted in the inset of Figure 4a.

Next, NEXAFS spectra were also obtained for the same two preparations on Cu(111) already discussed in the XPS section, where isolated intact species are dominating at $T_{\text{ann}} = 200$ K (Figure 4b) and deprotonated molecules within close-packed

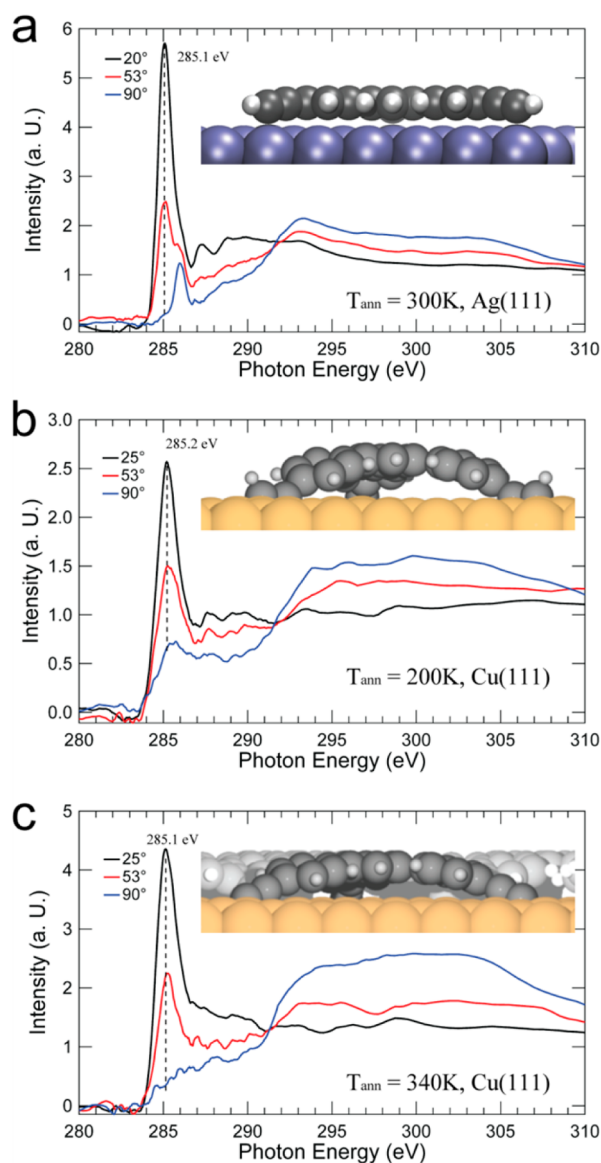


Figure 4. NEXAFS spectra at three angles, θ , of X-ray incidence with respect to the surface of the C K-edge of a (sub)monolayer Ext-TEB (a) on Ag(111), $T_{\text{ann}} = 300$ K, (b) on Cu(111), $T_{\text{ann}} = 200$ K, and (c) on Cu(111), $T_{\text{ann}} = 340$ K. Insets depict side views of the DFT-optimized adsorption geometries. (a. U.) represents arbitrary units.

islands are the majority species at $T_{\text{ann}} = 340$ K (Figure 4c). For both cases, the dichroism is reduced compared to the Ag case, the spectroscopic features are significantly broadened, and the alkyne-related structure, which was very prominent in the 90° spectrum of the previous sample (Figure 4a), is missing. These changes indicate distorted conformations due to chemisorption driven by the functional groups and thus confirm the picture suggested by the DFT calculations (insets). Since for such strong substrate interaction, the comparison to the single-molecule StoBe calculation is not applicable anymore and no functional group-specific features can be resolved, the broad feature at approximately 285 eV was fitted with a single peak and attributed solely to phenyl-related resonances, whereby possible minor contributions originating from the terminal moieties are neglected. For $T_{\text{ann}} = 200$ K, the evaluation of the angle-dependence (Figure S9b of the Supporting Information) results in an average tilt angle with respect to the surface of 30° .

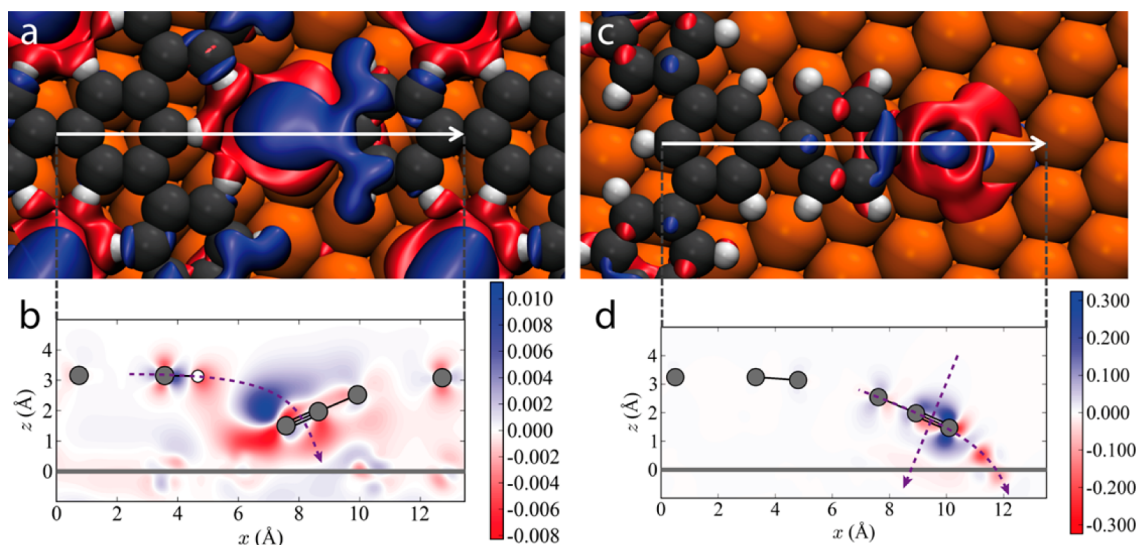


Figure 5. Electron density difference plots of deprotonated Ext-TEB on Cu(111) for the (a and b) network and (c and d) isolated case. (a) Top view of the electron density redistribution induced by molecule–molecule interaction as calculated by eq 2. The absolute value of the contours is $0.001 e/\text{\AA}^3$. (b) Cross section in the xz plane, where the x axis gives the distance along the white arrow in (a) and the z axis indicates the vertical distance to the surface. (c) Top view of the electron density redistribution induced by metal–molecule interaction of an isolated molecule. The absolute value of the contours is $0.005 e/\text{\AA}^3$. (d) Cross section in the xz plane, where the x axis gives the distance along the white arrow in (c). Blue indicates electron accumulation and red electron depletion. The units of the color bars are in $e/\text{\AA}^3$.

After annealing to 340 K, the dichroism of the π^* resonance is increased (Figure 4c), and its angle-dependence now provides an average tilt angle of 20° (Figure S9c of the Supporting Information). To link the experimental findings to the DFT optimized models, we calculated the average tilt angle of the phenyl moieties of the computed Ext-TEB/Cu(111) adsorption geometries (cf. Table S1 of the Supporting Information). Even though the absolute values depend on the type of averaging and are generally smaller than the experimental ones (for details see Supporting Information), the inferred flattening upon deprotonation of the molecular backbone by 5° to 6° agrees well with the experimental findings, further corroborating the deprotonation-driven self-assembly scenario.

DFT Study of the Nature of the Intermolecular Interactions. For a more detailed characterization of the close-packed supramolecular structure and the prevailing interactions, further DFT calculations were carried out. First, we discuss in more detail the network formation energy which is defined as

$$E_{\text{form}} = E(\text{network, sub}) - E(\text{Cu}_{\text{network}}) - [E(\text{isolated, sub}) - E(\text{Cu}_{\text{isolated}})] \quad (1)$$

where $E(\text{network, sub})$ is the total energy of the network on the substrate (sub) (note that each unit cell contains one molecule), $E(\text{Cu}_{\text{network}})$ is the total energy of the pristine relaxed Cu(111) surface used in the calculation of the network, $E(\text{isolated,sub})$ is the total energy of the isolated molecule on the substrate, and $E(\text{Cu}_{\text{isolated}})$ is the total energy of the pristine relaxed Cu(111) substrate used in the calculations of the isolated molecule. As mentioned before, the resulting formation energy is 0.04 eV/molecule and $-0.26 \text{ eV/molecule}$ for the intact and the deprotonated network, respectively, where the negative value denotes stabilization with respect to the reference system (an isolated molecule on the surface). The values for the formation energies depend sensitively on the sampling of the first Brillouin zone (referred to as k -point

sampling), see Figure S10 of the Supporting Information. Importantly, the often employed approximation of sampling only the Gamma-point is far from providing acceptable results. Here, careful convergence tests demonstrated that a dense k -point sampling is needed for sufficiently converged energies, required for obtaining valuable insight into the assembly energetics. Furthermore, also the molecular adsorption induced surface adaptation was specifically taken into consideration. The surface corrugation in the case of the deprotonated network is found to be similar to that in the isolated deprotonated case (Figure S11 of the Supporting Information), and the Cu(111) surface deformation energies for these two cases were calculated to be 0.36 (isolated) and 0.30 eV (network), respectively (Figure S11 of the Supporting Information). Therefore, this small difference ensures that the network formation energy E_{form} is mainly a reflection of the molecule–molecule bonding strength. For a 1,3,5-triethynylbenzene network on Ag(111), the corresponding value of $-0.11 \text{ eV/molecule}^{29}$ is smaller, suggesting the presence of a qualitatively different intermolecular interaction.

To investigate the bonding characteristics in the deprotonated Ext-TEB network, we considered a $p(2 \times 2)$ unit cell and calculated the electron density difference as

$$\Delta\rho_{\text{mol}} = (\rho_{\text{full}} - \rho_{\text{Cu}}) - (\rho_{\text{mol1@Cu}} + \rho_{\text{mol2@Cu}} + \rho_{\text{mol3@Cu}} + \rho_{\text{mol4@Cu}} - 4\rho_{\text{Cu}}) \quad (2)$$

where ρ_{full} is the electron density of the full molecule–surface system, ρ_{Cu} is the electron density of the clean Cu(111) surface (frozen in the geometry of the full system), and $\rho_{\text{mol}n\text{@Cu}}$ is the electron density of the n th molecule on the Cu(111) surface (frozen in the geometry of the full system). Within this definition, $\Delta\rho_{\text{mol}}$ gives the electron redistribution arising exclusively from molecule–molecule interactions. All (sub)structures were kept frozen in the geometry of the network on the surface. The resulting electron density difference plots are reproduced in Figure 5 and illustrate that the electron

redistribution is concentrated around the terminal alkynyls and neighboring C–H moieties. In earlier theoretical studies,^{58–60} it has been shown that for D–H···A type hydrogen bonding, a typical sequence of charge gain and loss regions is established. From the proton donor atom D to the proton acceptor atom A, it is expected to find electron gain, loss, gain, loss, gain, loss, gain, loss.⁵⁹ In Figure 5 depicting $\Delta\rho_{\text{mol}}$ the pattern observed along the dashed line is σ -like electron gain, π -like loss, σ -like gain, σ -like loss, π -like gain, π -like loss, π -like gain (with only faint blue color, shortly after the triple covalent bond axis), π -like loss. Thus, we classify the interaction as an ionic hydrogen bond between a C–H moiety of a phenyl ring (proton donor) and the π -system of the alkynyl group (proton acceptor). Since the downward tilting alkynyl group is interacting with C–H moieties of three surrounding aromatic rings at the same time (Figure 5a), the binding motif is identified as a trifurcated hydrogen bond.¹⁴ With the nonplanar conformation, the distances between the bonding terminal carbon atom and the three protons adopt reasonable values of ~ 3 Å, as visualized in Figure S12 of the Supporting Information. The van der Waals contribution to the intermolecular interaction was also addressed and found to be relative small compared to IHB, as shown in Figure S13 of the Supporting Information. C–H··· π ionic hydrogen bonds are known in 3D chemistry, however, for the reported cases, the ionic contribution is on the proton donor methine side (C–H⁺··· π),⁶¹ while in our case, the charge is contributed from the proton acceptor side (C–H··· π [–]), which option exists only in very specific clusters under ion solvation.⁶² We argue that this motif was not observed in 3D crystal engineering because the radical deprotonated alkynyl group is rather unstable and requires the metal support for its stabilization as provided in the current system. An additional feature of $\Delta\rho_{\text{mol}}$ is the electron depletion (red area, Figure 5b) between the alkynyl and the surface, which injects electrons into the intermolecular bond (deep blue area above the alkynyl end C atom, Figure 5b). We interpret this as a weakening of the molecule–surface interaction characteristic of an isolated adsorbed molecule that strengthens the molecule–molecule interaction. This interpretation is also supported by the fact that the terminal carbon atom, which can be seen as a formal radical, is lifted by 0.1 Å as a result of the network formation. Notice that the electron rearrangement due to the intermolecular interactions is restricted locally to the area around the bonding motif, and there is no sign of electron donation into the π -system of the aromatic backbone, thus no clear indication of proton acceptor ring interaction⁶³ is found in the current system.

According to the DFT calculated network formation energy, the binding energy of a single trifurcated ionic hydrogen bond amounts to $E_{\text{bind}} = -E_{\text{form}}/3 = 0.086$ eV (2 kcal/mol) and thus is relatively weak. Therefore, the room-temperature stability of the assemblies cannot result dominantly from intermolecular interactions, but a significant contribution must arise from the anchoring of the adsorbates to the Cu substrate.^{64,65} To address this point, an electron density difference plot reflecting the molecule–substrate interaction was calculated by $\Delta\rho_{\text{mol}} = \rho_{\text{mol}@Cu} - \rho_{Cu} - \rho_{\text{mol}}$ and is represented in Figure 5 (panels c and d). It can be clearly seen that a chemical bond is established between the alkynyl and surrounding Cu atoms (Figure 5d, curved arrow). In contrast to the charge difference patterns for typical σ -type molecule–substrate bonds reported before,^{43,64,65} here a larger volume is influenced. The electron density redistribution is located at both C atoms of the alkynyl,

and additional bonding directed from the alkynyl π -system to the substrate (Figure 5d, straight arrow) can be identified. Thus, we interpret the total bonding as a combined σ - and π -type interaction responsible for the strong anchoring of the carbon-only functional group. It should be further noticed that spin-polarized calculations could confirm that the unpaired spin of the alkynyl is quenched due to the interaction with the surface, manifesting the chemical nature of the molecule–substrate bond.

General Expression of IHB Motif. To demonstrate the generality of this novel binding motif, 9,10-diethynyl-anthracene (DEAN, Scheme 1b) was de novo synthesized, as described in the Supporting Information. Figure 6a shows an

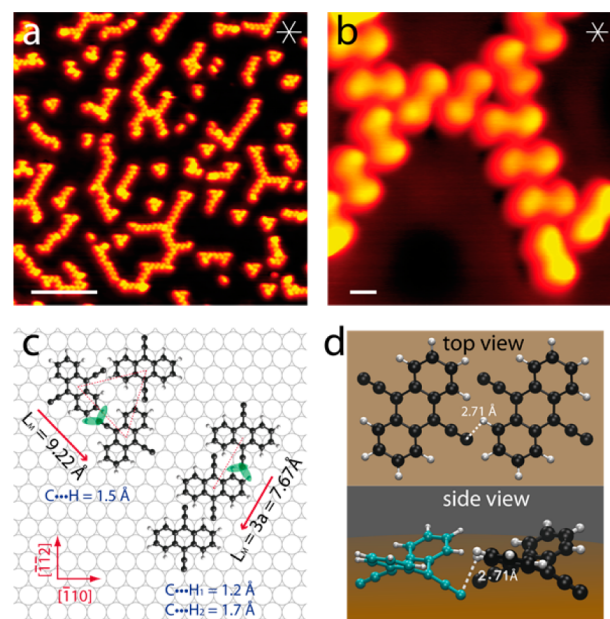


Figure 6. (a) STM image of 9,10-diethynyl-anthracene deposited on Cu(111) and annealed to 400 K, recorded at 5.5 K. ($U_b = -0.95$ V, $I_t = 0.1$ nA.) Scale bar denotes 50 Å. (b) Zoom-in image of the self-assembled supramolecular structure. ($U_b = -1.0$ V, $I_t = 0.08$ nA.) Scale bar denotes 10 Å. (c) Model of DEAN trimeric cluster and chain with planar gas phase model calculated by HYPERCHEM. (d) Proposed geometry of DEAN molecules upon adsorption on the Cu(111) surface. The anthracene coordinates are taken from ref 83, and the coordinates of the alkyne are adopted from the HYPERCHEM gas phase model of Ext-TEB.

overview image of a submonolayer sample prepared at 220 K on Cu(111) and annealed to 400 K. Molecular chains along the close-packed directions of the substrate are observed. Beside the chains, triangular clusters formed by three molecules are present. In the high-resolution image depicted in Figure 6b, a single molecule is imaged as two bright protrusions connected by a thin waist, with the long axis of the molecule aligned along the close-packed directions. Models in Figure 6c were constructed from the high-resolution experimental data (Figure S14 of the Supporting Information). Similar to Ext-TEB on Cu(111), the short distances between the C atoms from alkynyl and the neighboring H atoms of the phenyl rings (green ellipses in Figure 6c) indicate the deprotonation of the terminal alkyne. Moreover, the self-assembled structure is reminiscent of that formed by anthraquinone molecules on Cu(111).⁶⁶ To explain the extremely short IHB distances, we suggest a downward tilting of the terminal alkyne group toward the Cu surface

(Figure 6d), similar to Ext-TEB (Figure 2, Figure S12 of the Supporting Information) and the possible upward bending of the outer phenyl rings away from the surface.⁶⁷ Therefore, the distance of the shortest contact is 2.71 Å in the proposed distorted geometry (Figure 6d), larger than that in the flat-lying one (Figure 6c).

To verify the noncovalent nature of the self-assembled structures, lateral molecular manipulation was carried out. In Figure S15 of the Supporting Information, we show that both the triangular molecular clusters and the molecular chains can be disassembled by STM manipulation procedures demonstrating their supramolecular nature. Moreover, the DEAN dimer can be translated as a unit, in agreement with the expected strength of the IHB. In contrast to Ext-TEB, further heating up to 500 K did not trigger the formation of covalent structures, instead most of the molecules desorbed, and only a small amount of clusters remained on the surface.

CONCLUSION

The thermally activated deprotonation of terminal alkynes to yield surface-stabilized functional moieties opens up interesting novel possibilities for the formation and engineering of 2D supramolecular structures. In our prototypical study employing hydrocarbon species, well-defined 0D, 1D, and 2D nanosystems resulted from the hitherto unexplored alkynyl driven intermolecular forces. Our systematic investigation unraveled the nature of the new noncovalent interaction to be the first reported C–H $\cdots\pi$ - δ -type ionic hydrogen bond on surfaces. Experimental and theoretical results indicate high potential as construction tools for the realization of robust noncovalent nanoarchitectures due to the enhanced bonding strength in comparison to conventional H bonds involving carbon species and additional chemical bonding between the alkynyl group and the surface. This is especially important in the timely context of bottom-up construction of advanced hydrocarbon scaffolds⁶⁸ related to graphyne or graphdiyne,^{69,70} where alkynyl species could help to preorganize reactive monomers in well-defined initial situation for 2D polymerization under kinetic control.⁷¹ Notably, alkynes played a central role for both the preorganization of the supramolecular crystal as well as the polymerization reaction itself in recent pioneering work on the organic synthesis of 2D polymers by rational design.⁷² Also they unfolded their potential in the context of on-surface synthesis for the fabrication of extended graphdiyne molecular wires via vicinal surface templating.⁷³ Thus, our findings not only deepen the understanding of supramolecular chemistry and demonstrate the extended prospects provided by metallic supports, but they also offer a promising, novel tool for bottom-up construction of carbon-based nanomaterials.

METHODS

Synthesis. 1,3,5-Tris(4-ethynylphenyl)benzene (**1**)⁵¹ and 9,10-diethynyl-anthracene (**2**) were obtained by the coupling of correspondent aryl bromides and trimethylsilylacetylene (TMSA) or (triisopropylsilyl)acetylene (TIPSA) in the presence of the catalytic system copper(I)iodide/bis-(triphenylphosphine)palladium(II) dichloride and secondary amine as base. The resulting Si-contained intermediates were hydrolyzed to yield 86% and 75% of (**1**) and (**2**), respectively. Synthetic details are given in the Supporting Information.

Sample Preparation. All molecular systems and the clean metal surfaces were prepared in situ in UHV. The clean

Cu(111) and Ag(111) surfaces were prepared by repeated cycles of Ar⁺ sputtering and annealing to 740–800 K. Both types of molecules have been sublimated by organic molecular beam epitaxy from a quartz crucible inside a Knudsen cell. The Ext-TEB molecules were deposited by heating the crucible to 420–450 K. The 9,10-diethynyl-anthracene molecules were sublimated at 575 K. Ext-TEB molecules were dosed onto the clean Cu(111) surface held at 110 K, and subsequent annealing to 200 K was performed to desorb impurities.

STM Experiments. The STM measurements were carried out in two UHV systems with base pressure better than 2×10^{-10} mbar with a home-built Besocke-type STM or a commercial Joule-Thomson STM (SPECS GmbH). The unit cell parameters were obtained by averaging images of the same area with four different slow scanning directions to minimize the error due to drift. The unit cell orientation with respect to the substrate can be determined by atomically resolving the Cu(111) at the same temperature (5.5 K).

XPS and NEXAFS Experiments. The XPS and NEXAFS data were recorded at the HE-SGM monochromator dipole magnet beamline at the BESSY II synchrotron radiation source in Berlin, which provides light with a linear polarization of 90%. Photoelectrons were collected using a Scienta R3000 electron energy analyzer. C 1s spectra were acquired using an excitation energy of 435 eV, in normal emission and at a sample temperature of 200 K. The binding energy scale was calibrated against the Cu 3p_{3/2} line at 75.1 eV, and a Shirley background was subtracted from all spectra presented here.

For the NEXAFS measurements at the C K-edge, we used the partial electron yield mode of detection with a retarding voltage of 150 V. The NEXAFS spectra were acquired at 130 and 200 K for Ext-TEB on Ag(111) and on Cu(111), respectively, and referenced against a characteristic peak in simultaneously recorded spectra of a contaminated Au grid. Following a standard procedure, the signal of the bare crystal was subtracted from the raw data, which were subsequently corrected for the transmission through the beamline and the edge jump was normalized to 1.

DFT Calculations. Periodic density functional theory calculations were performed using the VASP⁷⁴ code with the projector-augmented wave method^{75,76} to describe ion-core interactions. The van der Waals density functional (vdW-DF)⁷⁷ described all nonlocal correlation, while local correlation was described by LDA and semilocal exchange by an optimized form of the Becke 86 functional.⁷⁸ The so-called optB86b/vdW-DF functional was recently shown to accurately describe adsorption of organic molecules on Cu(111).⁷⁹ In all calculations, a kinetic energy cutoff of 500 eV was used. The Cu(111) surfaces were described by 4-layered slabs separated by 15 Å of vacuum. If not stated otherwise, for the adsorption of isolated Ext-TEB molecules, a $p(9 \times 9)$ Cu(111) surface unit cell was used with a 6×6 k -point sampling. For the network, the unit cell determined experimentally was used together with a 9×9 k -point sampling. A convergence analysis with respect to k -point sampling has been included in the Supporting Information.

Simulated core-level shifts were obtained by comparing total energy differences between core-ionized and ground state systems. The total energies of core-ionized systems were computed by using a core-ionized PAW potential for the core-ionized atom as described by Köhler and Kresse.⁸⁰ The molecular orbital projected density of states was calculated by projecting the electronic states of a fully interacting system onto

the electronic states of an isolated state.⁸¹ STM images were simulated using the Tersoff-Hamann approximation,⁸² as implemented by Lorente and Persson.

HYPERCHEM Calculations. The molecular models of EXT-TEB and DEAN were optimized with semiempirical methods using the AM1 model implemented in the HYPERCHEM software (HYPERCHEM, Hypercube Inc., Gainesville, FL).

■ ASSOCIATED CONTENT

📄 Supporting Information

Details of the synthesis, STM images, statistical analysis, DFT calculations, NEXAFS spectra simulations, angle dependence analysis, phenyl ring tilt angles, convergence with respect to *k*-point sampling, analysis of surface corrugation, and analysis of van der Waals contribution. This material is available free of charge via the Internet at <http://pubs.acs.org>.

■ AUTHOR INFORMATION

Corresponding Author

*E-mail: florian.klappenberger@tum.de.

Author Contributions

¹Y.-Q.Z. and J.B. contributed equally to this work.

Notes

The authors declare no competing financial interest.

■ ACKNOWLEDGMENTS

Funding provided by the European Union via ERC Advanced Grant MolArt (Grant 247299), German Research Foundation (DFG) via BA 3395/2-1, KL 2294/3-1, and PP 1459 "Graphene" is gratefully acknowledged. Computational resources were allocated at the National Supercomputer Centre, Sweden, through SNAC and the MATTER consortium. We thank the Helmholtz-Zentrum Berlin for the allocation of synchrotron radiation beamtime and for financial support. We are grateful to Michael Naboka and Alexei Nefedov for technical assistance and support during the synchrotron experiments and to Christof Wöll for kindly providing access to the HE-SGM end station.

■ REFERENCES

- (1) Barth, J. V.; Costantini, G.; Kern, K. Engineering Atomic and Molecular Nanostructures at Surfaces. *Nature* **2005**, *437*, 671–679.
- (2) Barth, J. V. Molecular Architectonic on Metal Surfaces. *Annu. Rev. Phys. Chem.* **2007**, *58*, 375–407.
- (3) Elemans, J. A. A. W.; Lei, S. B.; De Feyter, S. Molecular and Supramolecular Networks on Surfaces: From Two-Dimensional Crystal Engineering to Reactivity. *Angew. Chem., Int. Ed.* **2009**, *48*, 7298–7332.
- (4) Bartels, L. Tailoring Molecular Layers at Metal Surfaces. *Nat. Chem.* **2010**, *2*, 87–95.
- (5) Palma, C. A.; Samori, P. Blueprinting Macromolecular Electronics. *Nat. Chem.* **2011**, *3*, 431–436.
- (6) Koepf, M.; Cherioux, F.; Wytko, J. A.; Weiss, J. 1D and 3D Surface-Assisted Self-Organization. *Coord. Chem. Rev.* **2012**, *256*, 2872–2892.
- (7) Klappenberger, F. Two-Dimensional Functional Molecular Nanoarchitectures—Complementary Investigations with Scanning Tunneling Microscopy and X-Ray Spectroscopy. *Prog. Surf. Sci.* **2014**, *89*, 1–55.
- (8) Böhringer, M.; Morgenstern, K.; Schneider, W. D.; Berndt, R.; Mauri, F.; De Vita, A.; Car, R. Two-Dimensional Self-Assembly of Supramolecular Clusters and Chains. *Phys. Rev. Lett.* **1999**, *83*, 324–327.

- (9) Barth, J. V.; Weckesser, J.; Cai, C. Z.; Günter, P.; Bürgi, L.; Jeandupeux, O.; Kern, K. Building Supramolecular Nanostructures at Surfaces by Hydrogen Bonding. *Angew. Chem., Int. Ed.* **2000**, *39*, 1230–1234.

- (10) Yokoyama, T.; Yokoyama, S.; Kamikado, T.; Okuno, Y.; Mashiko, S. Selective Assembly on a Surface of Supramolecular Aggregates with Controlled Size and Shape. *Nature* **2001**, *413*, 619–621.

- (11) Theobald, J. A.; Oxtoby, N. S.; Phillips, M. A.; Champness, N. R.; Beton, P. H. Controlling Molecular Deposition and Layer Structure with Supramolecular Surface Assemblies. *Nature* **2003**, *424*, 1029–1031.

- (12) Faul, C. F. J.; Antonietti, M. Ionic Self-Assembly: Facile Synthesis of Supramolecular Materials. *Adv. Mater.* **2003**, *15*, 673–683.

- (13) Meot-Ner, M. The Ionic Hydrogen Bond. *Chem. Rev.* **2005**, *105*, 213–284.

- (14) Steiner, T. The Hydrogen Bond in the Solid State. *Angew. Chem., Int. Ed.* **2002**, *41*, 48–76.

- (15) Aakeroy, C. B.; Beatty, A. M. Crystal Engineering of Hydrogen-Bonded Assemblies: A Progress Report. *Aust. J. Chem.* **2001**, *54*, 409–421.

- (16) Huyghues-Despointes, B. M. P.; Baldwin, R. L. Ion-Pair and Charged Hydrogen-Bond Interactions between Histidine and Aspartate in a Peptide Helix. *Biochemistry* **1997**, *36*, 1965–1970.

- (17) Lacroix, E.; Viguera, A. R.; Serrano, L. Elucidating the Folding Problem of Alpha-Helices: Local Motifs, Long-Range Electrostatics, Ionic-Strength Dependence and Prediction of NMR Parameters. *J. Mol. Biol.* **1998**, *284*, 173–191.

- (18) Huynh, M. H. V.; Meyer, T. J. Proton-Coupled Electron Transfer. *Chem. Rev.* **2007**, *107*, 5004–5064.

- (19) Zundel, G. *Hydrogen Bonds with Large Proton Polarizability and Proton Transfer Processes in Electrochemistry and Biology* In *Adv. Chem. Phys.*; John Wiley & Sons, Inc.: New York, 2000; Vol. *111*, pp 1–217.

- (20) Stepanow, S.; Strunskus, T.; Lingenfelder, M.; Dmitriev, A.; Spillmann, H.; Lin, N.; Barth, J. V.; Wöll, C.; Kern, K. Deprotonation-Driven Phase Transformations in Terephthalic Acid Self-Assembly on Cu(100). *J. Phys. Chem. B* **2004**, *108*, 19392–19397.

- (21) Cañas-Ventura, M. E.; Klappenberger, F.; Clair, S.; Pons, S.; Kern, K.; Brune, H.; Strunskus, T.; Wöll, C.; Fasel, R.; Barth, J. V. Coexistence of One- and Two-Dimensional Supramolecular Assemblies of Terephthalic Acid on Pd(111) due to Self-Limiting Deprotonation. *J. Chem. Phys.* **2006**, *125*, 184710-1–184710-8.

- (22) Ruben, M.; Payer, D.; Landa, A.; Comisso, A.; Gattinoni, C.; Lin, N.; Collin, J. P.; Sauvage, J. P.; De Vita, A.; Kern, K. 2D Supramolecular Assemblies of Benzene-1,3,5-triyl-tribenzoic Acid: Temperature-Induced Phase Transformations and Hierarchical Organization with Macrocyclic Molecules. *J. Am. Chem. Soc.* **2006**, *128*, 15644–15651.

- (23) Payer, D.; Comisso, A.; Dmitriev, A.; Strunskus, T.; Lin, N.; Wöll, C.; Devita, A.; Barth, J. V.; Kern, K. Ionic Hydrogen Bonds Controlling Two-Dimensional Supramolecular Systems at a Metal Surface. *Chem.—Eur. J.* **2007**, *13*, 3900–3906.

- (24) Pawlak, R.; Clair, S.; Oison, V.; Abel, M.; Ourdjini, O.; Zwaneveld, N. A. A.; Gignes, D.; Bertin, D.; Nony, L.; Porte, L. Robust Supramolecular Network on Ag(111): Hydrogen-Bond Enhancement through Partial Alcohol Dehydrogenation. *ChemPhysChem* **2009**, *10*, 1032–1035.

- (25) Bebensee, F.; Svane, K.; Bombis, C.; Masini, F.; Klyatskaya, S.; Besenbacher, F.; Ruben, M.; Hammer, B.; Linderroth, T. Adsorption and Dehydrogenation of Tetrahydroxybenzene on Cu(111). *Chem. Commun.* **2013**, *49*, 9308–9310.

- (26) Schiffrin, A.; Riemann, A.; Auwärter, W.; Pennec, Y.; Weber-Bargioni, A.; Cvetko, D.; Cossaro, A.; Morgante, A.; Barth, J. V. Zwitterionic Self-Assembly of L-Methionine Nanogratings on the Ag(111) Surface. *Proc. Natl. Acad. Sci. U.S.A.* **2007**, *104*, 5279–5284.

- (27) Schiffrin, A.; Reichert, J.; Pennec, Y.; Auwärter, W.; Weber-Bargioni, A.; Marschall, M.; Dell'Angela, M.; Cvetko, D.; Bavdek, G.; Cossaro, A.; et al. Self-Assembly of L-Methionine on Cu(111):

Steering Chiral Organization by Substrate Reactivity and Thermal Activation. *J. Phys. Chem. C* **2009**, *113*, 12101–12108.

(28) Li, Q.; Han, C. B.; Horton, S. R.; Fuentes-Cabrera, M.; Sumpter, B. G.; Lu, W. C.; Bernholc, J.; Maksymovych, P.; Pan, M. H. Supramolecular Self-Assembly of π -Conjugated Hydrocarbons via 2D Cooperative CH/ π Interaction. *ACS Nano* **2012**, *6*, 566–572.

(29) Kepčija, N.; Zhang, Y.-Q.; Kleinschrodt, M.; Björk, J.; Klyatskaya, S.; Klappenberger, F.; Ruben, M.; Barth, J. V. Steering On-Surface Self-Assembly of High-Quality Hydrocarbon Networks with Terminal Alkynes. *J. Phys. Chem. C* **2013**, *117*, 3987–3995.

(30) Cirera, B.; Zhang, Y.-Q.; Klyatskaya, S.; Ruben, M.; Klappenberger, F.; Barth, J. V. 2D Self-Assembly and Catalytic Homo-Coupling of the Terminal Alkyne 1,4-bis(3,5-diethynyl-phenyl)butadiyne-1,3 on Ag(111). *ChemCatChem* **2013**, *5*, 3281–3288.

(31) Nishio, M. CH/ π Hydrogen Bonds in Crystals. *CrystEngComm* **2004**, *6*, 130–158.

(32) Nishio, M.; Umezawa, Y.; Honda, K.; Tsuboyama, S.; Suezawa, H. CH/ π Hydrogen Bonds in Organic and Organometallic Chemistry. *CrystEngComm* **2009**, *11*, 1757–1788.

(33) Nishio, M. The CH/ π Hydrogen Bond in Chemistry. Conformation, Supramolecules, Optical Resolution and Interactions Involving Carbohydrates. *Phys. Chem. Chem. Phys.* **2011**, *13*, 13873–13900.

(34) Pennec, Y.; Auwärter, W.; Schiffrin, A.; Weber-Bargioni, A.; Riemann, A.; Barth, J. V. Supramolecular Gratings for Tuneable Confinement of Electrons on Metal Surfaces. *Nat. Nanotechnol.* **2007**, *2*, 99–103.

(35) Tomba, G.; Stengel, M.; Schneider, W. D.; Baldereschi, A.; De Vita, A. Supramolecular Self-Assembly Driven by Electrostatic Repulsion: The 1D Aggregation of Rubrene Pentagons on Au(111). *ACS Nano* **2010**, *4*, 7545–7551.

(36) Fraxedas, J.; García-Gil, S.; Monturet, S.; Lorente, N.; Fernández-Torrente, I.; Franke, K. J.; Pascual, J. I.; Vollmer, A.; Blum, R.-P.; Koch, N.; et al. Modulation of Surface Charge Transfer through Competing Long-Range Repulsive versus Short-Range Attractive Interactions. *J. Phys. Chem. C* **2011**, *115*, 18640–18648.

(37) Bischoff, F.; Seufert, K.; Auwärter, W.; Joshi, S.; Vijayaraghavan, S.; Ēcija, D.; Diller, K.; Papageorgiou, A. C.; Fischer, S.; Allegretti, F.; et al. How Surface Bonding and Repulsive Interactions Cause Phase Transformations: Ordering of a Prototype Macrocyclic Compound on Ag(111). *ACS Nano* **2013**, *7*, 3139–3149.

(38) Sohn, Y.; Wei, W.; White, J. M. Phenylacetylene on Cu(111): Adsorption Geometry, Interfacial Electronic Structures and Thermal Chemistry. *J. Phys. Chem. C* **2007**, *111*, 5101–5110.

(39) Treier, M.; Pignedoli, C. A.; Laino, T.; Rieger, R.; Müllen, K.; Passerone, D.; Fasel, R. Surface-Assisted Cyclodehydrogenation Provides a Synthetic Route Towards Easily Processable and Chemically Tailored Nanographenes. *Nat. Chem.* **2011**, *3*, 61–67.

(40) Duncan, D. A.; Bradley, M. K.; Unterberger, W.; Kreikemeyer-Lorenzo, D.; Lerotholi, T. J.; Robinson, J.; Woodruff, D. P. Deprotonated Glycine on Cu(111): Quantitative Structure Determination by Energy-Scanned Photoelectron Diffraction. *J. Phys. Chem. C* **2012**, *116*, 9985–9995.

(41) Papageorgiou, A. C.; Fischer, S.; Reichert, J.; Diller, K.; Blobner, F.; Klappenberger, F.; Allegretti, F.; Seitsonen, A. P.; Barth, J. V. Chemical Transformations Drive Complex Self-Assembly of Uracil on Close-Packed Coinage Metal Surfaces. *ACS Nano* **2012**, *6*, 2477–2486.

(42) Fischer, S.; Papageorgiou, A. C.; Lloyd, J. A.; Oh, S. C.; Diller, K.; Allegretti, F.; Klappenberger, F.; Seitsonen, A. P.; Reichert, J.; Barth, J. V. Self-Assembly and Chemical Modifications of Bisphenol A on Cu(111): Interplay Between Ordering and Thermally Activated Stepwise Deprotonation. *ACS Nano* **2014**, *8*, 207–215.

(43) Vitali, L.; Levita, G.; Ohmann, R.; Comisso, A.; De Vita, A.; Kern, K. Portrait of the Potential Barrier at Metal-Organic Nanocontacts. *Nat. Mater.* **2010**, *9*, 320–323.

(44) Ohmann, R.; Levita, G.; Vitali, L.; De Vita, A.; Kern, K. Influence of Subsurface Layers on the Adsorption of Large Organic

Molecules on Close-Packed Metal Surfaces. *ACS Nano* **2011**, *5*, 1360–1365.

(45) Lauhon, L. J.; Ho, W. Control and Characterization of a Multistep Unimolecular Reaction. *Phys. Rev. Lett.* **2000**, *84*, 1527–1530.

(46) Lauhon, L. J.; Ho, W. Inducing and Observing the Abstraction of a Single Hydrogen Atom in Bimolecular Reactions with a Scanning Tunneling Microscope. *J. Phys. Chem. B* **2001**, *105*, 3987–3992.

(47) Jung, T. A.; Schlittler, R. R.; Gimzewski, J. K. Conformational Identification of Individual Adsorbed Molecules with the STM. *Nature* **1997**, *386*, 696–698.

(48) Auwärter, W.; Klappenberger, F.; Weber-Bargioni, A.; Schiffrin, A.; Strunskus, T.; Wöll, C.; Pennec, Y.; Riemann, A.; Barth, J. V. Conformational Adaptation and Selective Adatom Capturing of Tetrapyrrolyl-Porphyrin Molecules on a Copper (111) Surface. *J. Am. Chem. Soc.* **2007**, *129*, 11279–11285.

(49) Tseng, T. C.; Urban, C.; Wang, Y.; Otero, R.; Tait, S. L.; Alcami, M.; Ēcija, D.; Trelka, M.; Gallego, J. M.; Lin, N.; et al. Charge-Transfer-Induced Structural Rearrangements at Both Sides of Organic/Metal Interfaces. *Nat. Chem.* **2010**, *2*, 374–379.

(50) Diller, K.; Klappenberger, F.; Marschall, M.; Hermann, K.; Nefedov, A.; Wöll, C.; Barth, J. V. Self-Metalation of 2H-Tetraphenylporphyrin on Cu(111): An X-Ray Spectroscopy Study. *J. Chem. Phys.* **2012**, *136*, 014705–1–13.

(51) Zhang, Y.-Q.; Kepčija, N.; Kleinschrodt, M.; Diller, K.; Fischer, S.; Papageorgiou, A. C.; Allegretti, F.; Björk, J.; Klyatskaya, S.; Klappenberger, F.; et al. Homo-Coupling of Terminal Alkynes on a Noble Metal Surface. *Nat. Commun.* **2012**, *3*, 1286–1–1286–8.

(52) Kung, H.; Wu, S. M.; Wu, Y. J.; Yang, Y. W.; Chiang, C. M. Tracking the Chemistry of Unsaturated C₃H₃ Groups Adsorbed on a Silver Surface: Propargyl-Allenyl-Acetylide Triple Bond Migration, Self-Hydrogenation, and Carbon-Carbon Bond Formation. *J. Am. Chem. Soc.* **2008**, *130*, 10263–10273.

(53) Battocchio, C.; Fratoddi, I.; Vitaliano, R.; Russo, M. V.; Polzonetti, G. Binuclear Pd(II) Complexes with Alkynyl Ligands and Functionalised Tail-Groups: Molecular and Electronic Structure Studied by XPS and EXAFS. *Solid State Sci.* **2010**, *12*, 1881–1885.

(54) Hermann, K.; Pettersson, L. G. M. Deprotonated Alkynyl Hydrogen Bonding in Metal-Surface-Supported Hydrocarbon Assemblies. *StoBe Software V. 3.0*, deMon developers group: Berlin and Stockholm, 2007 (<http://www.fhi-berlin.mpg.de/KHsoftware/StoBe>).

(55) Piantek, M.; Miguel, J.; Krüger, A.; Navío, C.; Bernien, M.; Ball, D. K.; Hermann, K.; Kuch, W. Temperature, Surface, and Coverage-Induced Conformational Changes of Azobenzene Derivatives on Cu(001). *J. Phys. Chem. C* **2009**, *113*, 20307–20315.

(56) Zhang, W. H.; Nefedov, A.; Naboka, M.; Cao, L.; Wöll, C. Molecular Orientation of Terephthalic Acid Assembly on Epitaxial Graphene: NEXAFS and XPS Study. *Phys. Chem. Chem. Phys.* **2012**, *14*, 10125–10131.

(57) Diller, K.; Klappenberger, F.; Allegretti, F.; Papageorgiou, A. C.; Fischer, S.; Wiengarten, A.; Joshi, S.; Seufert, K.; Ēcija, D.; Auwärter, W.; et al. Investigating the Molecule-Substrate Interaction of Prototypic Tetrapyrrole Compounds: Adsorption and Self-Metalation of Porphine on Cu(111). *J. Chem. Phys.* **2013**, *138*, 154710–1–154710–9.

(58) Yamabe, S.; Morokuma, K. Molecular-Orbital Studies of Hydrogen-Bonds 0.9. Electron-Distribution Analysis. *J. Am. Chem. Soc.* **1975**, *97*, 4458–4465.

(59) Kerns, R. C.; Allen, L. C. Cyclic and Bifurcated Hydrogen-Bonds. *J. Am. Chem. Soc.* **1978**, *100*, 6587–6594.

(60) Kelly, R. E. A.; Lee, Y. J.; Kantorovich, L. N. Homopairing Possibilities of the DNA Base Adenine. *J. Phys. Chem. B* **2005**, *109*, 11933–11939.

(61) Lee, J. Y.; Lee, S. J.; Choi, H. S.; Cho, S. J.; Kim, K. S.; Ha, T. K. Ab-Initio Study of the Complexation of Benzene with Ammonium Cations. *Chem. Phys. Lett.* **1995**, *232*, 67–71.

(62) Meot-Ner, M. The Ionic Hydrogen Bond and Ion Solvation. 7. Interaction Energies of Carbanions with Solvent Molecules. *J. Am. Chem. Soc.* **1988**, *110*, 3858–3862.

(63) Arras, E.; Seitsonen, A. P.; Klappenberger, F.; Barth, J. V. Nature of the Attractive Interaction between Proton Acceptors and Organic Ring Systems. *Phys. Chem. Chem. Phys.* **2012**, *14*, 15995–16001.

(64) Bieri, M.; Nguyen, M.-T.; Gröning, O.; Cai, J. M.; Treier, M.; Ait-Mansour, K.; Ruffieux, P.; Pignedoli, C. A.; Passerone, D.; Kastler, M.; et al. Two-Dimensional Polymer Formation on Surfaces: Insight Into the Roles of Precursor Mobility and Reactivity. *J. Am. Chem. Soc.* **2010**, *132*, 16669–16676.

(65) Nguyen, M.-T.; Pignedoli, C. A.; Passerone, D. An *Ab Initio* insight into the Cu(111)-Mediated Ullmann Reaction. *Phys. Chem. Chem. Phys.* **2011**, *13*, 154–160.

(66) Pawin, G.; Wong, K. L.; Kwon, K. Y.; Bartels, L. A Homomolecular Porous Network at a Cu(111). *Science* **2006**, *313*, 961–962.

(67) Kwon, K.-Y.; Wong, K. L.; Pawin, G.; Bartels, L.; Stolbov, S.; Rahman, T. S. Unidirectional Adsorbate Motion on a High-Symmetry Surface: “Walking” Molecules Can Stay the Course. *Phys. Rev. Lett.* **2005**, *95*, 166101–1–4.

(68) Diederich, F.; Kivala, M. All-Carbon Scaffolds by Rational Design. *Adv. Mater.* **2010**, *22*, 803–812.

(69) Ivanovskii, A. L. Graphynes and Graphdienes. *Prog. Solid State Chem.* **2013**, *41*, 1–19.

(70) Li, Y. J.; Xu, L.; Liu, H. B.; Li, Y. L. Graphdiyne and Graphyne: From Theoretical Predictions to Practical Construction. *Chem. Soc. Rev.* **2014**, *43*, 2572–2586.

(71) Colson, J. W.; Dichtel, W. R. Rationally Synthesized Two-Dimensional Polymers. *Nat. Chem.* **2013**, *5*, 453–465.

(72) Kissel, P.; Erni, R.; Schweizer, W. B.; Rossell, M. D.; King, B. T.; Bauer, T.; Götzinger, S.; Schlüter, A. D.; Sakamoto, J. A Two-Dimensional Polymer Prepared by Organic Synthesis. *Nat. Chem.* **2012**, *4*, 287–291.

(73) Cirera, B.; Zhang, Y.-Q.; Björk, J.; Klyatskaya, S.; Chen, Z.; Ruben, M.; Barth, J. V.; Klappenberger, F. Synthesis of Extended Graphdiyne Wires by Vicinal Surface Templating. *Nano Lett.* **2014**, *14*, 1891–1897.

(74) Kresse, G.; Furthmüller, J. Efficient Iterative Schemes for *Ab Initio* Total-Energy Calculations Using a Plane-Wave Basis Set. *Phys. Rev. B* **1996**, *54*, 11169–11186.

(75) Blöchl, P. E. Projector Augmented-Wave Method. *Phys. Rev. B* **1994**, *50*, 17953–17979.

(76) Kresse, G.; Joubert, D. From Ultrasoft Pseudopotentials to the Projector Augmented-Wave Method. *Phys. Rev. B* **1999**, *59*, 1758–1775.

(77) Dion, M.; Rydberg, H.; Schröder, E.; Langreth, D. C.; Lundqvist, B. I. Van der Waals Density Functional for General Geometries. *Phys. Rev. Lett.* **2004**, *92*, 246401–246404.

(78) Klimeš, J.; Bowler, D. R.; Michaelides, A. Van der Waals Density Functionals Applied to Solids. *Phys. Rev. B* **2011**, *83*, 195131–195143.

(79) Björk, J.; Stafstrom, S. Adsorption of Large Hydrocarbons on Coinage Metals: A van der Waals Density Functional Study. *ChemPhysChem* **2014**, *15*, 2851–2858.

(80) Köhler, L.; Kresse, G. Density Functional Study of CO on Rh(111). *Phys. Rev. B* **2004**, *70*, 165405–165413.

(81) Lorente, N.; Persson, M. Theoretical Aspects of Tunneling-Current-Induced Bond Excitation and Breaking at Surfaces. *Faraday Discuss.* **2000**, *117*, 277–290.

(82) Tersoff, J.; Hamann, D. R. Theory and Application for the Scanning Tunneling Microscope. *Phys. Rev. Lett.* **1983**, *50*, 1998–2001.

(83) Zade, S. S.; Zamoshchik, N.; Reddy, A. R.; Fridman-Marueli, G.; Sheberla, D.; Bendikov, M. Products and Mechanism of Acene Dimerization. A Computational Study. *J. Am. Chem. Soc.* **2011**, *133*, 10803–10816.